International Journal of Nanomedicine

Dovepress
Taylor & Francis Group

Open Access Full Text Article

ORIGINAL RESEARCH

3D-Printed PCL-Based Scaffolds with High Nanosized Synthetic Smectic Clay Content: Fabrication, Mechanical Properties, and Biological Evaluation for Bone Tissue Engineering

André SA Furtado[1,*], Manuel HS Cunha[1,*], Luciana MR Sousa[1], Guilherme C Brito[1], Thiago FCL Verde[1], Livia Alves Filgueiras[2], Leonardo A Sobral-Silva[3], Moisés V Santana[1], Gustavo F Sousa[1], Francisco EP Santos[4], Anderson N Mendes[2], José Figueredo-Silva[5], Antônio LM Maia Filho[5], Fernanda R Marciano[1,4], Luana MR Vasconcellos[3], Anderson O Lobo[1]

[1]Interdisciplinary Laboratory for Advanced Materials (LIMAV), Materials Science and Engineering Graduate Program (PPGCM), Federal University of Piauí (UFPI), Teresina, PI, Brazil; [2]Laboratory of Innovation in Science and Technology, Department of Biophysics and Physiology, Federal University of Piauí, Teresina, PI, Brazil; [3]Institute of Science and Technology, São Paulo State University (UNESP), São Paulo, SP, Brazil; [4]Department of Physics, Federal University of Piauí (UFPI), Teresina, PI, Brazil; [5]Biotechnology Research Center - State University of Piauí, Teresina, PI, Brazil

*These authors contributed equally to this work

Correspondence: Anderson O Lobo, Interdisciplinary Laboratory for Advanced Materials, UFPI - Federal University of Piauí, Teresina, Brazil, Email lobo@ufpi.edu.br

Background: The 3D printing of macro- and mesoporous biomimetic grafts composed of polycaprolactone (PCL) infused with nanosized synthetic smectic clay is a promising innovation in biomaterials for bone tissue engineering (BTE). The main challenge lies in achieving a uniform distribution of nanoceramics across low to high concentrations within the polymer matrix while preserving mechanical properties and biological performance essential for successful osseointegration.

Methods: This study utilized 3D printing to fabricate PCL scaffolds enriched with nanosized synthetic smectic clay (LAP) to evaluate its effects on structural, chemical, thermal, mechanical, and degradative properties, with a focus on in vitro biological performance and non-toxicity. Scaffolds were created with varying proportions of PCL and LAP. Comprehensive characterization included scanning electron microscopy (SEM), X-ray diffraction (XRD), thermogravimetric analysis (TGA), Fourier-transform infrared spectroscopy (FTIR), mechanical testing, swelling analysis, and degradation studies. Biological performance was assessed through MTT assays (cell viability), alkaline phosphatase activity, histological analysis, and Raman spectroscopy, highlighting the scaffolds' biocompatibility and potential applications in regenerative medicine.

Results: The developed inks demonstrated excellent injectability, and the 3D-printed PCL/LAP scaffolds exhibited a microporous and rough structure, good structural fidelity, low degradability, thermal stability, and sufficient mechanical strength across all formulations. Intrinsic properties of the scaffolds revealed no cytotoxicity while enhancing bioactivity and promoting in vitro mineralization when cultured with mesenchymal stem cells in all analyzed groups. Notably, the high concentration of LAP within the PCL matrices did not induce in vitro cytotoxicity but rather stimulated in vitro mineralization and differentiation.

Conclusion: This study demonstrated the feasibility of 3D printing PCL/LAP scaffolds with high concentrations of nanoceramics. Both in vitro and in vivo assays validated the regenerative potential of these scaffolds, emphasizing their efficacy as a promising approach for developing advanced biomimetic grafts.

Keywords: grafting, polycaprolactone, bone tissue regeneration, synthetic smectic clay

Received: 19 October 2024
Accepted: 18 December 2024
Published: 4 January 2025

Introduction

3D modeling for biomimetic transplants plays a pivotal role in advancing medical treatments for complex and challenging-to-regenerate tissue defects. The capability to customize patterns for bone defects is emerging as a promising approach for accelerating healing and propelling the field of bone tissue engineering (BTE). Polycaprolactone (PCL), a biocompatible and non-toxic polymer approved by the US Food and Drug Administration (FDA), can mimic the structural properties of bone tissue when processed through 3D printing.[1] However, enhancing the bioactivity of PCL often requires the incorporation of additional components into synthetic grafts, such as ceramics like synthetic smectic clay (LAP).[2] The use of 3D printing enables the exploration of high concentrations and novel ratios of scaffold components tailored for specific applications.[3] By enriching a PCL matrix with high concentrations of LAP, synthetic grafts for long bones, such as the tibia, can exceed mere structural reconstruction.[4] The bone marrow within these bones can benefit significantly from the ions and bioactive properties of LAP. In higher concentrations, LAP functions as both an immunomodulatory agent and a reservoir of essential bioactive ions, such as magnesium (Mg) and sodium (Na). These ions are critical for the proper functioning of cells involved in bone repair as well as the maintenance of bone marrow cellular activity. This enriched environment promotes not only efficient bone reconstruction but also the sustained functionality of the bone marrow during the healing process.[5,6]

The enrichment of polymeric biomaterials with nanofillers is a well-established practice to enhance their properties in the production of biomimetic grafts. Typically, the nanofiller content in such materials is relatively low compared to the overall polymer matrix, resulting in only modest improvements in key properties such as mechanical performance and bioactivity. Consequently, exploring the potential of materials enriched with high concentrations of silicates could unveil new opportunities for their application in bone tissue engineering (BTE).[7–9] In BTE, these challenges are addressed by developing materials that mimic the properties of the natural extracellular matrix of bone, particularly its structural components, such as scaffolds.[10,11] These scaffolds provide three-dimensional mechanical support for cells, facilitating the formation of new tissue at the defect site. To achieve effective osseointegration, scaffolds must exhibit good mechanical stability, biocompatibility, appropriate biodegradability, and osteoconductivity, while also being non-cytotoxic. The ability to rapidly and efficiently fabricate biofunctional synthetic grafts using customizable three-dimensional models, such as those created through 3D printing techniques, is emerging as a promising solution for addressing specific bone defects. This approach not only accelerates the production process but also allows for tailored treatments that align closely with the unique requirements of individual patients.[12–15]

Several studies have reported concentration-dependent effects of LAP on the properties of biomaterials. Cidonio et al demonstrated that increasing the silicate concentration in 3D-printed scaffolds composed of gelatin and LAP enhanced their mechanical properties. The study highlighted that both mechanical strength and the material's regenerative performance improved with higher LAP loading.[16] Similarly, Bin Liu et al observed an increase in viscosity and a reduction in hydration of hydrogels when composites contained a higher LAP concentration, specifically at 3% (w/v).[17] Dong et al further corroborated these findings, showing that 3D-printed hydrogels with 8% LAP exhibited enhanced mechanical properties, improved cell viability, and greater cell adhesion.[4] Their study also noted that the high nanofiller concentration increased surface roughness, promoting cell attachment and tissue adhesion. This enhancement contributed to improved in vitro biomineralization, a faster degradation rate, an increased crystallization temperature of PCL, and enhanced osteogenic differentiation of human mesenchymal stem cells (hMSCs) in electrospun scaffolds.[3,4] Despite these advancements, the concentration of LAP in the studies mentioned above remains relatively low compared to the polymeric matrix with which it is combined.[12,13,18] Many investigations limit LAP concentration to levels that do not compromise the printability of the material. For instance, Dong et al noted that increasing the LAP content from 8% to 10% in relation to gelatin necessitated adjustments to the needle diameter and printing speed to maintain resolution in 3D printing.[4] Xiongcheng Xu et al studied PCL scaffolds containing 5 wt% LAP, fabricated using fused deposition modeling (FDM), for oral and maxillofacial bone reconstruction. They found that LAP significantly enhanced the scaffolds' regenerative properties and their biomimetic resemblance to the target tissue.[19]

Chen, Khong, and Huang fabricated PCL scaffolds with an exceptionally high LAP concentration (30% w/v) using direct ink writing, characterizing them via X-ray micro-computed tomography (micro-CT). Their findings revealed that

this elevated LAP concentration not only maintained the final conformation of the printed material but also ensured good resolution. Moreover, a significant enhancement in mechanical strength was observed.[20] Building on these findings, this study aimed to fabricate and evaluate PCL scaffolds containing exponentially higher concentrations of LAP (20%, 33%, and 50% w/v) than typically reported in the literature for additive manufacturing via 3D printing. These proportions represent unprecedented levels of nanoclay enrichment in scaffolds. Despite the high LAP content, all groups were successfully produced with satisfactory resolution. The scaffolds were subsequently characterized and assessed for their bioactivity and biocompatibility, with the goal of identifying the most suitable concentration for applications in BTE. This exploration of extreme LAP loadings seeks to establish new parameters for scaffold design and expand the applicability of such materials in regenerative medicine.

Materials and Methods

Materials

Polycaprolactone (PCL, Mw 8×10^4 g/mol), Alizarin Red S purchased from Sigma-Aldrich (Sigma-Aldrich, St. Louis, USA), nanosized LAP (Laponite® acquired from BYK Additives Ltd., USA), Dichloromethane (DCM), Dibutyl phthalate (DBF) NaCl, $MgCl_2.6H_2O$, $CaCl_2.2H_2O$, Na_2HPO_4 and $NaHCO_3$ (NEON Inc. São Paulo BR). 10 mL syringes, 23G needles purchased from (BD Ultra-Fine), essential alpha MEM medium culture, gentamicin (500 µg / mL) (Gibco), 10% Bovine Fetal Serum (SBF) (LGC Technology, Campinas Brazil).

Preparation of Inks for 3D Printing

Table 1 summarizes the ink formulations investigated in this study, with preparation protocols adapted from Jakus et al. Liquid inks for 3D printing were formulated with varying proportions of PCL and LAP in a bisolvent system comprising dichloromethane (evaporative agent) and dibutyl phthalate (plasticizer) (Table 1). To prepare the inks, PCL (20% w/v) was dissolved in 4 mL of the bisolvent mixture (dichloromethane and dibutyl phthalate at a 4:1 v/v ratio) under magnetic stirring in a closed flask at room temperature until complete dissolution. Subsequently, LAP was added in different proportions, and the mixture was stirred further to achieve homogeneity. The resulting ink was transferred into a 10 mL syringe (Descarpack Inc)., and partial solvent evaporation was performed in a laboratory fume hood until the ink attained a viscosity suitable for 3D printing.

Manufacturing of Scaffolds

Before 3D printing the scaffolds, the models were created using CAD software and saved in STL format. Each model was designed with a square shape measuring 1×1 cm and featured a grid pattern, with alternating layers rotated by 90° on the z-axis at a thickness of 0.1 mm. Following the CAD design, the.STL file was processed in software to generate a. GCODE file, which is compatible with the 3D printer. During this conversion, various printing parameters, including print speed, layer height, filament diameter, and temperature, were configured. The.GCODE file and the syringe

Table 1 Summary of Compositions and Preparation of PCL/LAP Inks for 3D Printing

Group	Solid ratio Proportion (w/w)	LAP	PCL	Preparation
PCL	PCL: 100	0	100	Stirring at room temperature
PCLLAP41	PCL: 80 LAP: 20 4:1	20	80	
PCLLAP21	PCL: 66.6 LAP: 33.3 2:1	33.3	66.6	
PCLLAP11	PCL: 50 LAP: 50 1:1	50	50	

https://doi.org/10.2147/IJN.S497539

containing the PCL/LAP solution were then loaded into a 3D bioprinter (Allevi 2, Allevi Inc). Six samples were printed per session, each consisting of 20 layers and requiring approximately 30 minutes of printing time. Upon completion of the printing process, the scaffolds were washed with 70% alcohol and dried to remove any residual solvent.

Injectability Assay

To assess the injectability of the inks, a NanoMec50 – Hsensor compression tester was employed for each sample (N=3). The testing parameters matched those used during material printing, as detailed in Table 2 and Supplementary Video 1.

3D Scaffolding Characterization

Microscopic analysis of the scaffolds was conducted using scanning electron microscopy (SEM, FEI, Quanta FEG 250 model) with energy dispersive X-ray spectroscopy to examine their surface properties. For X-ray diffraction analysis, flat disks with a diameter of 15 mm and a height of 0.1 mm were produced. The analysis was performed with a Shimadzu XRD 6000 diffractometer using Cu Kα radiation (λ=1.5406 Å), and data were collected over a range of 5° to 75° at a scan rate of 2°/min for crystallinity analysis. Fourier transform infrared spectroscopy with attenuated total reflectance (FTIR-ATR; model Vertex 70, Bruker, Germany) was used to identify the functional groups in the scaffolds. Spectra were collected in the range of 4000 cm^{-1} to 600 cm^{-1}. Thermogravimetric analysis was carried out on the prepared scaffolds to assess their thermal stability. Thermogravimetric curves were obtained using the Shimadzu TGA-50 device, heating the samples to 1000 °C at a rate of 20°/min in an argon atmosphere. Compression tests (stress-strain curves of PCL and LAP at different concentrations) were performed on a texture analyzer (model TA.XT plus, Stable Micro Systems Ltd, Vienna, United Kingdom) equipped with a 5 kg load cell. Rectangular samples (10 x 10 mm and 20 layers) from each group were compressed at 25 °C with a strain rate of 1 mm/min (N=3 per group). The swelling capacity was determined by immersing scaffolds in PBS buffer solution (pH 7.4) at 36°C for 40 days. Swelling was calculated by weighing the scaffolds (N=3) before and after immersion in PBS (after 17 hours). Percent swelling was calculated as [(W1 – W0)/W0] x 100, where W1 is the weight of the swollen samples at regular intervals and W0 is the weight of the dry scaffold. The degradation of the composite scaffolds was evaluated by immersing them in PBS, with scaffold weights recorded at regular intervals after washing five times with water.

In vitro Testing

Cell Isolation

The in vitro tests were conducted in accordance with the ethical guidelines set by the National Council for the Control of Animal Experiments (CONCEA) and approved by the local ethics committee (process number 12/2020). Mesenchymal stem cells (MSC) were isolated from the femurs of nine Wistar rats (Rattus norvegicus). The femurs were purified in a laminar flow hood, and cell culture flasks (250 mL and 75 cm^2, TPP, Biosystems, Curitiba, Brazil) with essential alpha-MEM culture medium (Gibco) supplemented with 10% fetal bovine serum (LGC Technology, Campinas, Brazil) and gentamicin (500 μg/mL, Gibco) were used to maintain the bone marrow cells. The cells were incubated at 37°C with 5% CO_2. The culture medium was replaced every three days, and the cell growth was monitored using an inverted phase-contrast microscope (Carl Zeiss Axiovert 40C, Germany). Upon reaching confluence, the cells were enzymatically dissociated and seeded at a density of $1x10^2$ viable cells per well in a 96-well microplate (TPP, Biosystems, Curitiba, Brazil).[21] Prior to seeding, the wells were weighed and sterilized under UV light. Osteogenic culture medium was added to each well and changed every 48 hours. All plates were incubated at 37°C with 5% CO_2 until the time of testing. All experiments were conducted following the guidelines of ISO 10993–5.[22]

Table 2 3D Printing Parameters for PCL/LAP Scaffolds

Speed	Pressure	Layer Height	Needle (Ø)	Temperature
3 (mm/s)	30 ~ 40 (psi)	0.1 (mm)	23G (0.33 mm)	25°C

Cell Viability

After 3 days of culture, cell viability was quantitatively evaluated using the MTT assay. Cells were incubated with an MTT solution (3-(4,5-dimethylthiazol-2-yl)-2,5-diphenyltetrazolium bromide, Sigma-Aldrich) at 37°C for 4 hours, during which metabolically active cells reduced MTT to formazan crystals. Post-incubation, dimethyl sulfoxide (DMSO, Sigma-Aldrich) was added to each well to dissolve the crystals. The plates were then gently shaken at room temperature to ensure complete solubilization of the formazan. Absorbance was measured at 570 nm using a spectrophotometer (Micronal AJX 1900, São Paulo, Brazil). The absorbance values, derived from N = 5 per group, served as an indicator of cellular metabolic activity.

Alkaline Phosphatase Assay During MSC Differentiation

The activity of alkaline phosphatase (ALP) was assessed using a commercial kit (Labtest Diagnóstica, Minas Gerais, Brazil) following the manufacturer's protocol. Cell lysates were prepared by homogenizing the samples in an appropriate lysis buffer. ALP activity was determined by measuring the hydrolysis of thymolphthalein monophosphate. The reaction mixture was incubated at 37°C for the recommended duration, after which the reaction was terminated using the provided stopping solution. The release of thymolphthalein was quantified by measuring absorbance at 590 nm with a spectrophotometer (Micronal AJX 1900, São Paulo, Brazil). ALP activity was normalized to the total protein content in the same lysates, and statistical analysis was conducted using data from N = 5 per group.

Formation of Mineralization Nodules

After 14 days of culture, the formation of mineralization nodules was evaluated in the samples (n = 3) through Alizarin Red S staining to detect calcium deposition. Samples were fixed with 4% paraformaldehyde at room temperature for 15 minutes, rinsed with distilled water, and incubated in a 2% Alizarin Red S solution (Sigma-Aldrich, St. Louis, Brazil) adjusted to pH 4.2 for 20 minutes under gentle agitation. Excess dye was removed by thorough washing with distilled water until the rinse was clear, ensuring specific staining of calcium-rich regions. The stained samples were examined under an optical microscope (Axio Observer A1, Carl Zeiss, Germany). The presence of red-stained nodules confirmed calcium deposition, highlighting the osteogenic potential of the samples.

Statistical Analysis

All tests were initially subjected to the Kolmogorov–Smirnov test to assess normality, confirming data homogeneity ($p > 0.05$). In vitro assay results were analyzed using a two-way ANOVA ($p < 0.05$), with period and scaffold type as variables (N = 3). Data are expressed as mean ± standard deviation, and post hoc analysis was conducted using Tukey's test when required. All statistical analyses were performed using GraphPad Prism 6.0 software (GraphPad Software, San Diego, CA, USA). A significance level of 5% and a statistical power of 80% were adopted for all tests.

Biomineralization

A 5× SBF (Simulated Body Fluid) solution was prepared by dissolving NaCl (42.86 g), $MgCl_2.6H_2O$ (1.52 g), $CaCl_2.2H_2O$ (1.83 g), Na_2HPO_4 (0.70 g), and $NaHCO_3$ (1.76 g) in 1 L of distilled water in a polypropylene (PP) beaker. The pH of the solution was adjusted to 6.1 using HCl while stirring. Subsequently, 75 mL of the solution was distributed into four plastic containers. Three 1×1 cm samples, each with two layers of thickness from each group (N = 3), were immersed in 75 mL of the SBF solution. The containers were incubated at 37°C with gentle shaking at 80 rpm. The pH of the solution was monitored throughout the 7-day immersion period, during which no solution renewal was performed. After the incubation, the samples were retrieved for further analysis.

In vivo Assay

Wistar rats (*Rattus norvegicus*) were selected for the in vivo analysis. Healthy young adult rats were divided into two groups (n=3*n*=3 per group). After a 30-day experimental period, the animals were euthanized using an overdose of an

anesthetic combination of xylazine (10 mg/kg) and ketamine (80 mg/kg). The tibiae, including the bone defect area, were excised, fixed in 10% (v/v) neutral buffered formalin for 24 hours (pH 7.0), and decalcified in 10% EDTA for two weeks. Following decalcification, the specimens underwent routine histological processing using an automated tissue processor (PT05 TS Luptec, São Carlos, Brazil) and were embedded in paraffin. Longitudinal histological sections (5 μm thick) were prepared using a rotary microtome (MRP09 Luptec, São Carlos, Brazil) and stained with hematoxylin-eosin (H&E). Histological analysis was performed under an optical microscope (Olympus CX31, Tokyo, Japan) equipped with a digital camera (Moticam WiFi X, MoticMicroscopes, Richmond, VA, USA). Comparative descriptive analysis focused on the demarcation line between pre-existing bone and newly formed tissue at the cortical defect site. The in vivo tests adhered to ethical principles established by the National Council for the Control of Animal Experiments (CONCEA) and were approved by the Ethics Committee of the State University of Piauí (Registration No. 016195/2022-9).

Results and Discussion

Manufacturing and Characterization of 3D Scaffolding

Prior to 3D printing, injectability tests were conducted using various ink formulations (Figure 1). These tests confirmed the optimal parameters for 3D printing the prepared PCL/LAP inks. The evaluated parameters, which were employed during scaffold fabrication, are summarized in Table 2. The scaffolds were successfully fabricated using a solvent evaporation-based 3D printing process for PCL/LAP inks. The printed samples exhibited excellent structural fidelity, maintaining their designed geometry and integrity. Scaffolds were printed with up to 20 layers, each with a height of 0.1 mm, demonstrating precise control over layer-by-layer deposition (Figure S1).

The injectability tests confirmed the parameter adjustments required for the printability of each ink formulation. It was observed that the force needed to extrude the material through the needle is directly proportional to the concentration of LAP relative to the polymer in the ink (as detailed in the curves from Figure 1 and Supplementary Video 1, specifically for the PCLLAP41 group). Notably, the composition of the solutions can present challenges in other techniques for producing three-dimensional scaffolds. However, these challenges are mitigated in 3D printing due to the ability to adjust a wide range of parameters during the printing process or through software planning, thereby overcoming potential obstacles in the construction of the final product. Figure 1, derived from the compression of the inks, illustrates the homogeneity of each solution. The consistent increase in each curve up to the stability point confirms the appropriate dispersion of LAP. In contrast, a heterogeneous solution would exhibit abrupt increases in force followed by short decreases, indicative of alternating phases being expelled. The absence of such irregularities further supports the uniformity of the inks.[23]

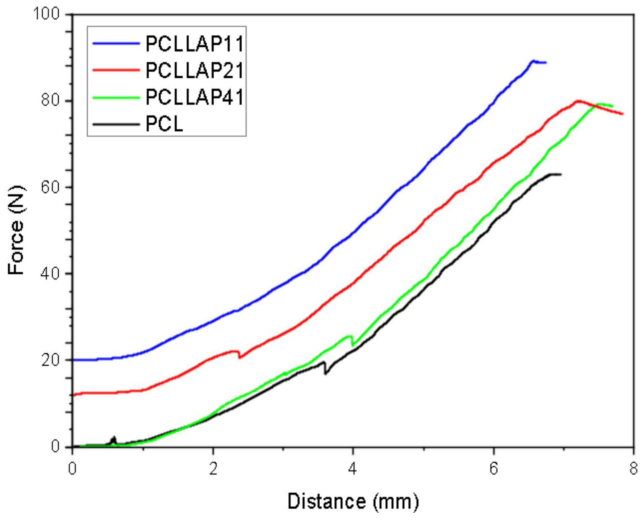

Figure 1 Injectability performance for each developed ink.

Morphological Characterization of PCL/LAP Scaffolds

The PCL/LAP composites were prepared in different ratios: 1:1, 2:1, and 4:1 (Figure S1). Figure 2(Ia) displays the drawn 3D structure, while Figure 2(IIa) illustrates the corresponding structure after 3D printing. All formulations exhibited high resolution during the 3D printing process (Figure 2a). The microscopic image corresponding to the most optimal PCL/LAP group (4:1 ratio) demonstrated the best fidelity when compared to the CAD design. Notably, the injectability test revealed that the force-to-distance ratio for this group was immediately higher than that for the pure PCL and slightly lower than that observed in the other LAP-treated groups (Figure 1). The appearance of the inks and all printed scaffold groups is provided in the supplementary materials (Supplementary Materials, Figure 1). The scaffold morphology was analyzed using scanning electron microscopy (SEM) to assess their structural features and dimensions (Figure 2b–e). The SEM images revealed typical three-dimensional porous structures, ideal for supporting cell growth (Figure 2b). The average size of the macropores across all groups was approximately 700 µm (Figure 2c). The scaffolds demonstrated a three-dimensional macroporous arrangement (Figure 2d), which closely mimics bone tissue, making them suitable for the temporary replacement of long bones, such as the tibia, which contains bone marrow. The voids in the material, if applied to a full transverse defect, would aid in accommodating the bone marrow, an essential tissue for blood cell production and containing a large population of undifferentiated cells in the latency phase. For optimal osseointegration, pores ranging from >50 µm to <1 mm are preferred, as they promote a better regenerative response (Figure 2d). Additionally, macroporosity facilitates cell colonization, as well as the penetration of blood vessels and microvessels, which are essential for nourishing newly formed tissue and enabling the scaffold's integration with the surrounding biological tissue (Figure 2e). [24,25]

Figure 2 Images of the scaffolds with the best fidelity (PCLLAP41 group). (a) I: CAD drawing of the scaffold, II: image of the final product obtained by 3D printing. SEM images showing (b) details of the arrangement and microporous structure, (c) visual roughness, (d) fidelity of the printed image, and (e) detailed view of the visual roughness of the PCLLAP41 group scaffolds at different magnifications.

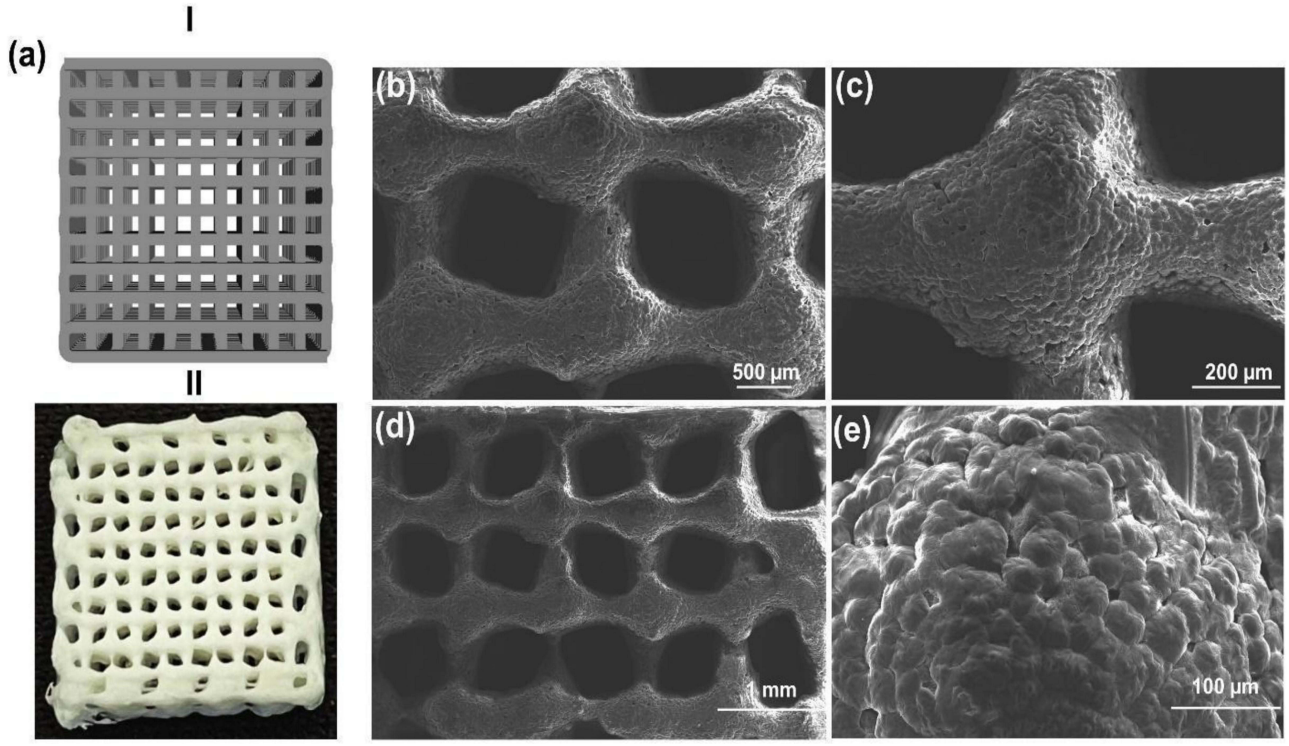

Figure 2 Images from the best fidelity scaffolds (PCLLAP41 group). (**a**) I represent the CAD drawing of the scaffolding, II image of the final product obtained by 3D printing. SEM image showing (**b**) details of arrangement and microporous structure, (**c**) visually roughness, (**d**) fidelity of printed image and (**e**) details of visually roughness scaffolds of PCLLAP 41 group at different magnifications.

https://doi.org/10.2147/IJN.S497539

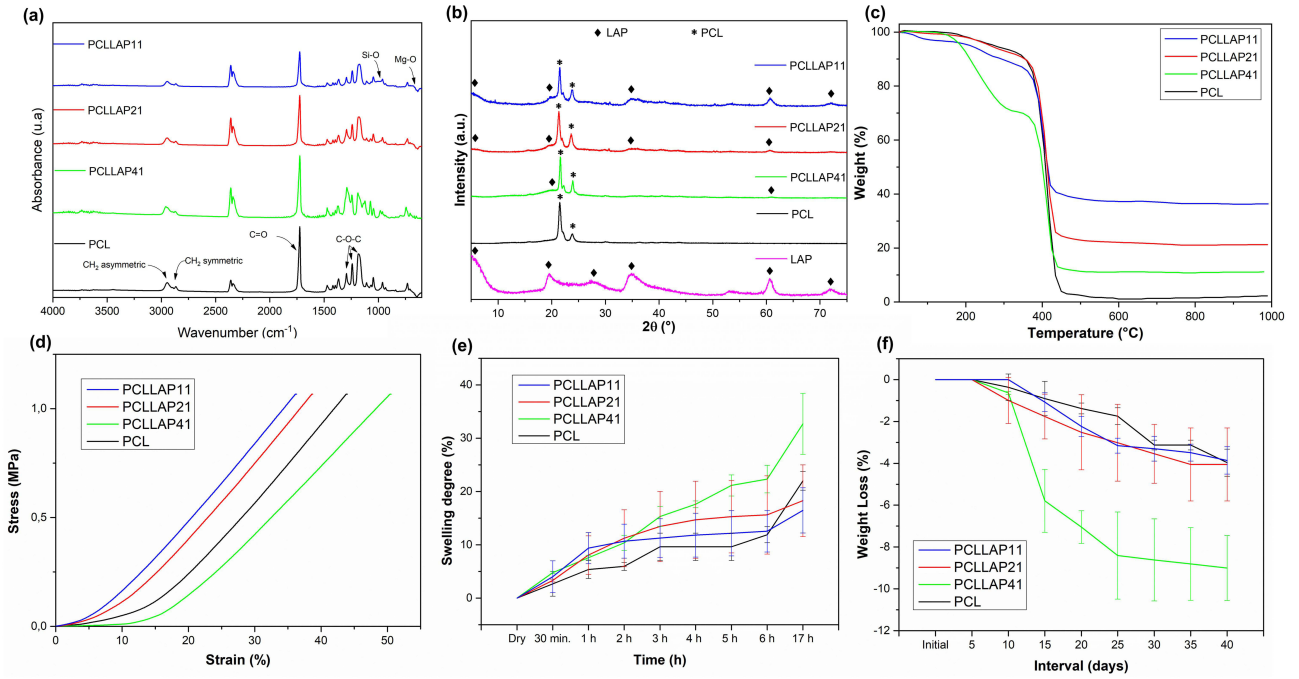

Figure 3 Characterization of scaffolds: (**a**) Fourier-transform infrared spectroscopy spectra of PCL scaffolds and PCL/LAP composites with varying LAP contents, highlighting the composition of the studied material. (**b**) X-ray diffraction pattern of PCL scaffolds, LAP, and PCL/LAP composites at different concentrations: 1:1, 2:1 and 4:1, showing the presence of two well-defined phases related to the precursor materials. (**c**) Thermogravimetric analysis (TG) of PCL scaffolds and PCL/LAP at different concentrations: 1:1, 2:1 and 4:1. (**d**) Tensile Test, (**e**) Swelling, and (**f**) Degradation studies.

Figure 3 shows all the results of the chemical and mineralogical characterization of the new framework composites. Figure 3a shows the FTIR spectra of PCL and PCLLAP41, PCLLAP21 and PCLLAP11 scaffolds. The spectra of all composites of the new scaffolds showed structural bands characteristic of PCL. The bands centered at 2945 cm^{-1} correspond to the asymmetric stretching of CH bonds in CH_2, while the bands at 2865 cm^{-1} correspond to the symmetric stretching of CH bonds in CH_2. The bands at about 1720 cm^{-1} are associated with the stretching of the C=O bonds in the ester groups, while the bands at 1294 cm^{-1}, 1240 cm^{-1} and 1162 cm^{-1} correspond to the stretching of the COC groups.[25] In the spectra of all analyzed groups, low intensity bands are observed in the 1009 cm^{-1} and 652 cm^{-1} regions, which are related to Si-O stretching and Mg-O deformation, respectively.[26] The coexistence of bands related to both PCL and LAP for all analyzed groups indicates the incorporation of nanosilicate into the polymeric matrix. Furthermore, the increase in LAP content is evidenced by the increase in the intensity of the bands related to this component. When LAP are present in PCLLAP11 group, these bands become clearer. The FTIR results confirm the XRD regarding the concentration of LAP in the samples. The diffraction peaks show higher intensity and more peaks associated with LAP when the samples contain a higher proportion of LAP[21,22] (Table 1), such as the PCLLAP41 and PCLLAP21. Figure 3b shows the X-ray diffraction pattern of pure LAP powder and the diffractograms of PCL scaffolds and PCL/LAP composites at different concentrations prepared by 3D printing. The diffractogram of the LAP powder shows peaks at angles of 19.8° and 27.6° of 2θ, confirming the nanocomposite coating.[25]

All scaffolds exhibited well-defined diffraction peaks at angles of 21.5° and 23.9° from 2θ, which were associated with the semi-crystalline structure of PCL.[27] In the PCL/LAP composites, in addition to the peaks associated with PCL, those associated with LAP are also observed, indicating the presence of two distinct phases. FTIR, XRD and EDS characterizations showed the LAP presence (specially PCLLAP11 and PCLLAP21 groups). The thermal stability and organic and inorganic content of the 3D printed scaffolds were evaluated by thermogravimetric analysis (Figure 3c) and the results showed good thermal stability up to a temperature of approximately 350 °C, where typical polyester decomposition occurs. Low mass loss was observed in the groups, which was related to moisture and residual solvent content, with the greatest mass loss occurring

in the PCLLAP41 group at around 200 °C. And at approx. 400 °C, a strong thermal decomposition can be observed in all groups examined, which is related to the degradation of PCL (typical for polyester, between 350 °C and 400 °C), after 500 °C the PCL sample is almost completely degraded. The content of residual solids in the PCLLAP41, PCLLAP21 and PCLLAP11 groups, which was 11.2%, 21.6% and 37%, respectively, is associated with the LAP component and showed good thermal stability up to 1000 °C.[28–30] The percentage of residue does not match the percentage originally used in the paint formulation, which reinforces the idea of the presence of moisture and/or solvent in the tested samples. The mechanical properties of scaffolds are important in BTE as the biomaterials must withstand dynamic mechanical loads for in vivo application. As shown, the effect of adding LAP to the manufactured scaffold was evaluated here using a compression test. Figure 3d shows the stress-strain curves of PCL and LAP scaffold at different aspect ratios. Analysis of the curves shows that all groups withstood a load of 1 MPa without plastic deformation, which means that the applied load returns to its original size after removal without permanent deformation.[31]

The scaffold, which consisted only of PCL, exhibited a deformation of 43.7% at the maximum observed stress of 1 MPa. The addition of LAP in different concentrations led to changes in the mechanical behavior of the material. The PCLLAP41 group showed a more ductile behavior than the group consisting only of printed PCL, as it deformed more under the same load and showed a deformation of 50.4% at the maximum stress of 1 MPa. The addition of LAP (PCLLAP11 and PCLLAP21) resulted in a stiffer scaffold than the processed groups of pure PCL and PCLLAP41, resulting in lower deformations at the maximum observed stress, 38.7% and 36.1% respectively. This is due to the addition of LAP, which provides greater mechanical resistance, as also shown in another study.[32] It is hypothesized that the addition of nanoparticles to a polymer matrix such as PCL improves the mechanical properties, for example by increasing stiffness, where the material deforms less under greater loads. However, this effect cannot always be verified, as was observed for all PCLLAP groups, as LAP can negatively influence the mechanical properties of the nanocomposites. Possibly, it should aggregate within the material and affect the elastic deformation,[25,27] justifying the slightly lower mechanical behavior observed in this group. At higher concentrations, 25 wt% and 50 wt%, as in the PCLLAP21 and PCLLAP11 groups, the mechanical properties increased, and the results suggest that the mechanical properties of PCL and LAP scaffolds can be modulated depending on the content of nanoparticles. Figure 3e–f shows the degree of swelling of the 3D-printed PCL and LAPscaffolds up to 17 hours after testing. The PCLLAP41 scaffold shows greater water absorption compared to the other groups. From this, we can conclude that this nanocomposite has a greater visual porosity that allows it to absorb more water than the others, as found in other studies.[33] Although LAP has a hydrophilic property, the scaffolds with a higher concentration of LAP (PCLLAP21 and PCLLAP11 scaffolds) showed similar water absorption to the scaffolds consisting of printed PCL only. Significant degradation was only observed in all groups after 15 days of testing. The PCL, PCLLAP21 and PCLLAP11 scaffolds showed a similar rate of degradation after 40 days, but the PCLLAP41 scaffold showed a higher rate of degradation. The degradation of PCL occurs mainly by hydrolytic cleavage of ester groups.[32,34] As a hydrophobic polymer, PCL tends to degrade slowly in aqueous environments such as physiological fluids. The superior degradation performance observed in the PCLLAP41 group can be attributed to a less uniform hydrolytic interaction within the scaffold structure compared to other groups. This results in degradation at specific points within the scaffold structure, increasing the material's surface area in contact with the medium and thereby enhancing hydrolysis.[33] LAP distributed in high concentrations may act as a physical barrier, reducing the polymeric matrix's surface contact with the medium and delaying its degradation. So, the stronger water adsorption observed in PCLLAP41 may have favored the degradation process of this group.[26] The degradability stimulated by LAP is a very important property for the applicability of the material as a biomimetic graft. When the material is implanted, it initially fills the defect and its mechanical properties, such as compressive strength, are crucial for good performance. Over time, however, this material must degrade to make room for the formation of resident tissue and eventually complete the graft. Therefore, the PCLLAP41 group is considered the best concentration of LAP for applications such as bone grafting due to its greater degradability.

Biological Tests

The deposition of apatite on the surface of materials during immersion in SBF is an indirect method to evaluate the potential in vivo bioactivity of new materials/scaffolds.[35] The fabricated scaffolds were immersed in SBF and apatite formation was evaluated by SEM and EDS analysis. Figure 4 shows the PCLLAP41 (more fidelity group) scaffold before

 https://doi.org/10.2147/IJN.S497539

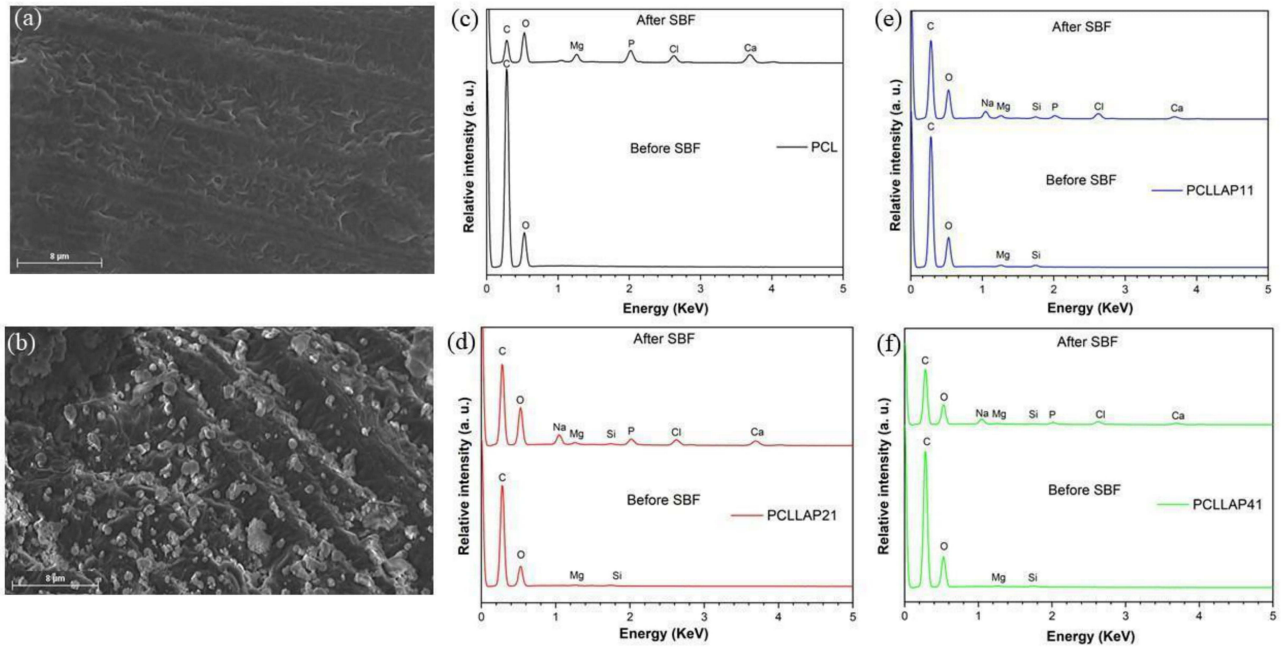

Figure 4 (**a**) Scanning electron microscopy of the 3D printed scaffold surface before SBF treatment, (**b**) Scanning electron microscopy of the scaffold surface after SBF treatment. (**c**) Dispersive energy diagram of the neat PCL sample to identify the elemental composition. In (**d**), (**e**) and (**f**); Dispersive energy diagram for the tested groups with high LAP load.

(Figure 4a) and after immersion in SBF (Figure 4b), showing the formation of particles on the surface of the material. Analysis by EDS (Figure 4c–f) confirms that the surface of the material has characteristic peaks of the elements P and Ca associated with apatite, as well as peaks associated with the constituents of PCL and LAP (EDS mapping analyses identified C, O, Mg, Si, Figure S2-S4). The SBF test gives an insight into what should happen to the material when implanted in the physiological environment. The deposition of apatite plays an important role in bone formation and maintenance. Apatite provides greater mechanical strength and rigidity to the outer layer of the bone, contributes to tissue mineralization so that the ions involved provide the necessary resistance to the deeper layers of the bone, and stores minerals that mediate the cellular activity of this tissue.[36]

LAP is already frequently used as an agent to improve the bioactivity of polymers for BTE. It is usually used in low concentrations such as 1%, 2% or 5% and is already an important factor in obtaining new properties for the receiving material.[17,37–40] When enriching a PCL matrix with high concentrations of LAP, the large ion supply and the chemical nature of the clay provide ideal conditions for the rapid mineralization of the newly formed tissue and the maintenance of differentiated cells.[17,40–42]

The cytotoxicity of the 3D printed scaffolds was evaluated after three days using the MTT assay. The results showed that the PCL, PCLLAP21 and PCLLAP11 scaffolds had similar in vitro cytocompatibility compared to each other and to the control group ($p>0.05$), while the PCLLAP41 scaffolds had statistically higher cell viability than the others in the study ($p<0.05$), as shown in Figure 5a. These findings indicate that the addition of a high content of LAP does not have a negative effect on the cytotoxicity of the scaffolds, confirming the in vitro cytocompatibility, similar to other studies.[35,40,42–44] This fact can be explained due to the biocompatibility of PCL associated with biodegradation, that is, when it undergoes hydrolysis, it locally produces a small amount of acid that is not harmful to cells, and can also provide space for cell growth. Da Fonseca et al; Camarero-Espinosa et al, (2021). Gaharwar et al (2014) demonstrated that when nanoclay is added, the degradation rate of PCL increases, which significantly contributes to the interaction of the biomaterial with mesenchymal cells.[38–40] Results from in vitro tests analysis have shown that all analyzed groups were non-toxic in terms of cell viability when high loads of LAP were used. The concentration of material in the extracellular environment directly influences a cell's ability to differentiate and undergo mitosis or remain static and work more slowly.[45] Figure 5b shows that all

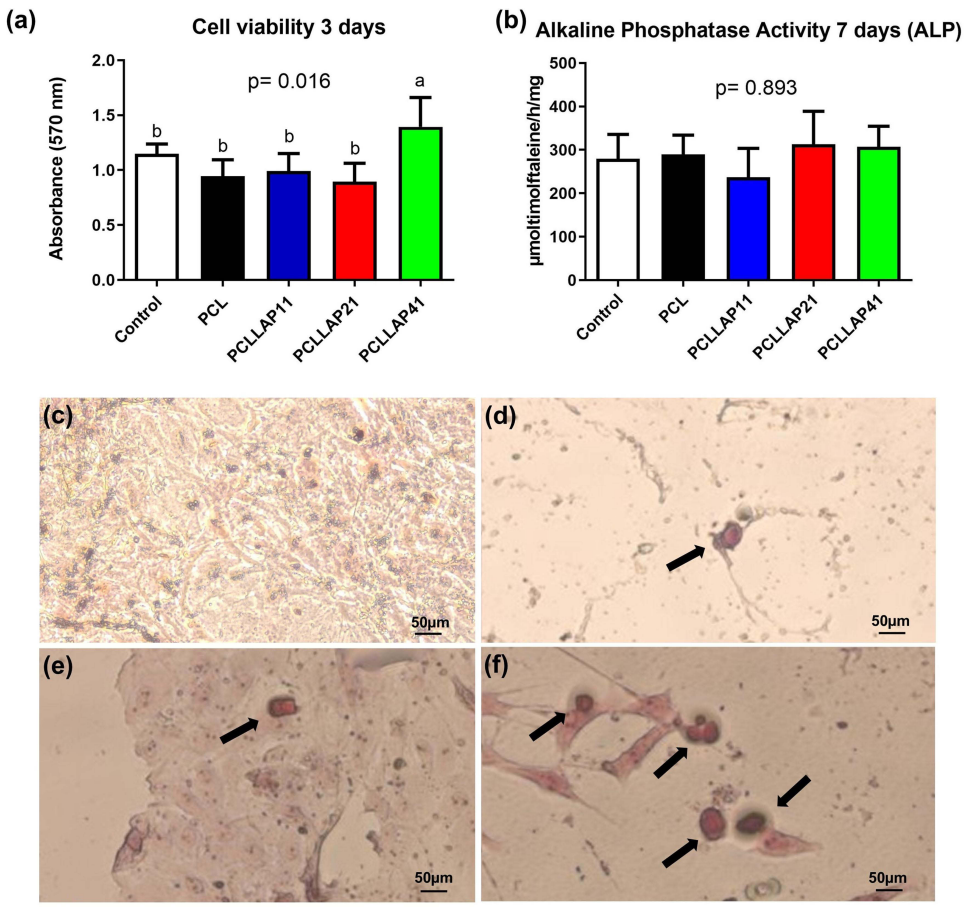

Figure 5 Graphics represent mean values (±) standard deviation (**a**) Cell viability after three days. (**b**) Alkaline phosphatase activity after seven days. (**c–f**) Mineralization nodules after 14 days arrows point to the nodules. (**c**) PCL, (**d**) 11, (**e**) 21 e (**f**) 41. Image of the formation of mineralization nodules Original magnification × 50 (scale bars = 50 µm). In vitro data presented as mean value ± standard, n=5, deviation analyzed by two-way ANOVA ($p<0.05$), subjected to Tukey's post-hoc test.
The authors changed this figure to change number formats from the "a" and "b".

groups performed well in terms of alkaline phosphatase activity. This indicates that the prepared material influenced the cellular differentiation process of mesenchymal stem cells into osteoblasts, which is in line with previous studies in the literature.[17,19] In the in vitro and in vivo investigation by Xu et al, a porous PCL structure incorporated in 3D printed LAP was evaluated with the aim of accelerating the osteogenesis of mesenchymal cells. This investigation showed that this biomaterial increased angiogenic gene expression and secretion of cytokines, in addition to expressing the activity of the alkaline phosphatase enzyme, suggesting a significant impact on osteogenic differentiation by producing extracellular proteins specifically related to bone. The activity of ALP, an important marker for osteogenic differentiation, indicates that the mesenchymal cells used in the study were able to differentiate into osteoblasts when they encountered the material.[46] It is important to emphasize that the PCLLAP41 group performs better with regard to the analysis of cell viability, as shown in Figure 5a. This parameter indicates a harmonious effect between the elements in the extracellular and intracellular environments, as well as a structural biofunctional effect due to the dispersion of LAP in the polymeric matrix, a factor that facilitates the proper activity of the cells within the synthetic tissue. The mineralization effect was observed in all the groups, as shown in Figure 5c–f, confirming the ability of LAP to induce undifferentiated cells to specialize into bone tissue, even at high concentrations.[47],Figure S5, demonstrates that there is no significant difference between the groups regarding the release of proteins by the seeded cells. Additionally, the hemolytic activity assay indicates that none of the tested concentrations exhibited toxicity to erythrocytes. When compared to PCL alone,

https://doi.org/10.2147/IJN.S497539

the addition of LAP improved cell differentiation in all tested groups and proved to be efficient in sustaining and supporting the formation of mineralized bone matrix, being a material with promising properties to be applied in tissue engineering. Recent in vivo experiments show that nanoclay-associated PCL scaffolds significantly promote vascular ingrowth and improve bone regeneration at the defect site.[48] The results of the present in vitro test demonstrate the ability of a personalized, high LAP-loaded biomaterial to promote osteoinductive bioactivity, showcasing significant potential for in vivo application in the treatment of critical defects. Additionally, a lower concentration of ceramic within the polymeric matrix can induce better porosity and permeability, acting as an adjuvant for effective nutrient diffusion between environments.

The deposition of inorganic calcium demonstrates the complete stabilization and maturation of the differentiated cells, determining the extent of mineralization of the previously analyzed groups.[38] In the alizarin red mineralization test, a dye that acts specifically on inorganic calcium, it was observed that nodule formation occurred in all groups tested with high concentration of LAP (Figure 5c–f). [41] High concentrations of the ceramic provide a larger number of ions in the extracellular matrix, which can stimulate osteoconduction when interacting with pluripotent cells. The inducing effect of LAP on cell differentiation is directly related to its chemical nature. By analyzing dispersion spectroscopy (see Figure 4 and Figures S2-S4), we can confirm the presence of magnesium and sodium in the samples, characteristic chemical elements of LAP. The magnesium present in LAP plays an important role in cell activity, mediating the cell's energy production via ATP and contributing directly to the activity of enzymes and proteins associated with general cell metabolism.[49] Sodium is important for electrolyte balance and contributes to the osmotic well-being of cells, while lithium acts as an important signaling agent through the composition of functional enzymes and proteins,[49,50] The formation of nodules in the PCLLAP11, PCLLAP21 and PCLLAP41 groups presented here, as well as ALP activity, indicate that LAP stimulates cells to differentiate into bone by the above mechanisms, confirming the suitability of the material for BTE. The enrichment of PCL with a high amount of LAP resulted in higher mechanical strength of the scaffold (Figure 3d), an important factor for mimicking bone that is initially incomplete and is filled by the implant. The cellular viability and osteoconductive properties act as a catalyst in the regeneration process and induce the resident cells, which may have been suppressed by microbial activity, to proliferate by mitosis and refill the defect. In addition, the porous structure of the material provides the necessary conditions for the attachment not only of bone cells but also of adjacent tissue that can contribute to the tissue regeneration process. It is important to emphasize that cellular activity is dependent on the microenvironment in which the cell is situated. As observed, a moderate load of LAP (20%) in the PCLLAP41 group provides a more favorable environment for satisfactory cellular activity compared to other groups. Furthermore, mechanical and degradation assays reinforce the enhanced viability of this proportion for direct applications in bone tissue mimicry. The increased swelling observed in the PCLLAP41 group may be justified by its evenly distributed, localized distribution within the scaffold structure, allowing for more uniform absorption effects.[33] Conversely, in more concentrated groups, LAP, being hydrophilic, may form a physical barrier that limits water interaction with the polymeric portion of the scaffold, which would also tend to swell.[32] The data analysis allows the understanding that the use of LAP as an adjuvant for improving polymeric scaffolds should be moderate. Although the in vitro analysis data indicate that all tested groups can be used for BTE, the sample group with lower LAP concentration (PCLLAP41) still stands out for demonstrating more satisfactory performance in both in vitro biological assays and structural characterization.

In vivo Testing

The histological findings after 30 days of evolution are shown in Figure 6. For the in vivo assays, two groups were tested: the PCLLAP41 group, due to its more promising possibilities among the groups containing nanoceramics, and the group based on pure PCL scaffolds to determine the differences related to regenerative capacity. Both groups showed intense fibrous thickening of the periosteum and new bone formation connecting the two edges of the bone defect. In the PCL group, the new, interconnected trabeculae were thin and irregular, containing relatively scarce osteoblasts randomly

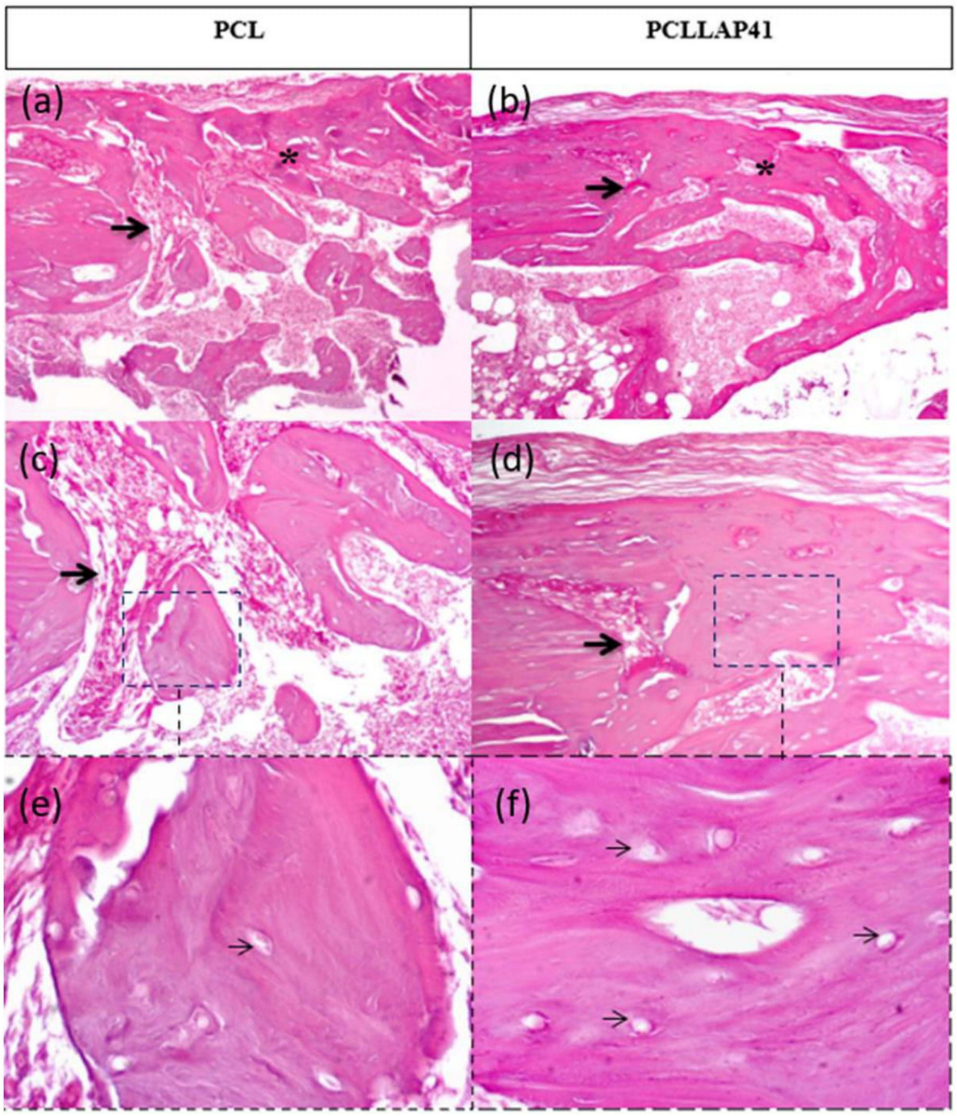

Figure 6 *Histological aspects after thirty days of evolution.* The larger arrows indicate the limit between the pre-existing cortical bone and the newly formed tissue in the cortical defect, "*" indicates mature Trabecular Bone. In the PCL group, the newly formed bone trabeculae (*) are smaller and irregular, containing scarce osteoblasts (small arrow) distributed in a poorly organized matrix. The PCL/LAP group exhibited numerous osteocytes (smaller arrows), distributed in a more organized matrix. Newly formed trabeculae (asterisks) are thicker and compact. (**a**), (**b**): 40x; (**c**), (**d**) 100x; (**e**), (**f**): 400x. (H&E).

distributed in a poorly organized matrix (Figures 6a, and e). In comparison, the group PCL/LAP exhibited bone neoformation with a more mature aspect. The newly formed trabeculae were thicker and contained a greater number of osteocytes distributed regularly in an apparently more organized matrix. However, well-defined osteons were not found. (Figure 6b,). Although the lamellar structure of normal cortical bone tissue has not been fully recovered, the results of the histological analysis showed that, for the period of 30 days, the combination of PCL and the LAP at high concentration induced the formation of new trabecular bone with more cellularity and mature areas. The process of osseointegration occurs through a complex sequence of events that begins at the moment of injury; initially, there is an inflammatory response aimed at recruiting growth factors and immune cells responsible for phagocytosing microorganisms, cellular debris, and loose inorganic fragments from the injury site. LAP is known for its immunomodulatory effects, capable of reducing excessive inflammation that could lead to graft rejection and shortening the duration of tissue inflammation, which is crucial as this period involves almost total loss of function at the injury site.[51] Following the formation of the soft callus, the nanoceramic acts as a reservoir of ions that serve as raw material for the bone mineralization process.[51,52] As observed in Figure 6f, there is a higher incidence of osteocytes embedded in the bone

https://doi.org/10.2147/IJN.S497539

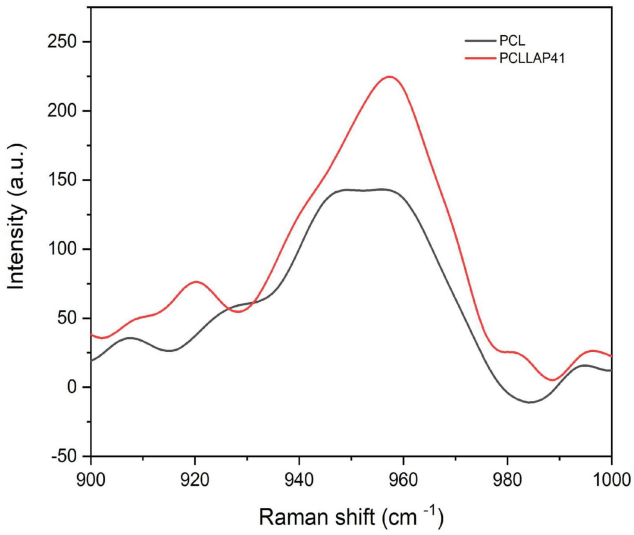

Figure 7 Raman spectroscopy of the defect region in the tibia after 30 days of graft exposure.

tissue in the sample containing a high concentration of LAP, indicating complete maturation of the region undergoing regeneration. Additionally, the LAP load may have influenced better osteocyte distribution and trabeculae formation through a mechanism of cellular affinity.[53] Furthermore, the greater homogeneity of mature bone tissue observed in the PCLLAP41 group indicates uniform deposition of collagen and mineralized extracellular matrix, leading to efficient recovery of tissue function and a favorable progression in the tissue regenerative process.[3,52,53] To complement the analysis of the regenerative process, Raman spectroscopy was performed on the surface of the defects after 30 days of grafting (Figure 7), comparing the intensity of the phosphate-related bands in each group. The presence of the phosphate function band was confirmed by the appearance of a band at 960 cm^{-1} (PO_4^{3-} stretching; 4) in both groups; however, a higher intensity was recorded in the PCLLAP41 group, indicating that the high concentration of the LAP effectively enhanced the tissue mineralization process.[54] During the regeneration process, osteoblasts are responsible for creating a mineralized inorganic matrix by depositing hydroxyapatite ($Ca_5(PO_4)_3(OH)$). Phosphate, as one of the main components of hydroxyapatite, is therefore found in abundance in functional bone tissue.[55] Table 3 provides an overview of the main studies published containing LAP as a nanofiller. It is noteworthy that in the present study, the concentrations of LAP tested in comparison to the polymer matrix are exponentially higher than in most of the previously published articles.

Table 3 Recent Studies Using LAP to Improve Scaffolds for Tissue Regeneration

Aimed Tissue	Polymeric Matrix	LAP Concentration	Manufacturing technique	References
Bone Tissue	**Polycaprolactone**	**20, 33 and 50%**	**3D printing**	**This Article**
Bone Tissue	Polycaprolactone	0.5, 2, and 3.5%	Electrospinning	Arab-Ahmadi et al (2020)[50]
Bone Tissue	Polylatic acid	0.4, 1.8 and 1.2%	Electrospinning	Orafa et al (2021)[56]
Bone Tissue	Polycaprolactone	1%	3D printing	Bonjun Cao et al (2023)[48]
Urethra Tissue	Polylatic acid-glycolic	0.1, 1 and 10%	Electrospinning	Wang et al (2020)[57]
Bone tissue	GelMA	8%	3D printing	Dong et al (2021)[4]
Bone tissue	Polycaprolactone	30%	3D printing	Chen H. et al (2021)[20]

Notes: Percentage of LAP in relation to the polymer matrix.
Abbreviations: PCL, Policaprolactone; LAP, synthetic smectic clay; BTE, Bone tissue engineering; hMSCs, human stem mesenchymal cells; DCM, Dichloromethane; FDM, fusion deposition modeling; SEM, scanning electron microscopy; SBF, Simulated Body Fluid; DRX, X-ray diffraction; FTIR, Fourier Transformed Infra-red spectroscopy; TG, thermogravimetry; SBF, simulated blood fluid, ALP, alkaline phosphatase; MSC, mesenchymal stem cell.

Conclusion

Herein we demonstrated the feasibility of 3D printing scaffolds based on the modeling of PCL by liquid deposition, where the proposed proportions of LAP into scaffolds for BTE are still rarely used. The injectability tests have shown that different loadings of LAP have no influence on the printability, as the applied forces are lower compared to the distance of the extruded inks. The scaffolds obtained exhibited good structural fidelity (specially PCLLAP41 group) regardless of the LAP concentration and showed an organized and multilayered structure. SEM analysis examined the surface of the fabricated scaffolds in all groups studied, while XRD confirmed the composition of the scaffolds and revealed two phases related to the initially proposed compositions of PCL and LAP. The 3D-printed scaffolds showed good thermal stability according to the thermogravimetric analysis. An improvement in the bioactivity of the material due to the high concentration of LAP dispersed in PCL was confirmed by mineralization tests and cell viability. Although in vitro study showed that the highest cell viability and differentiation index for the target tissue occurred at lower concentrations of LAP (PCLLAP41), the possibility of using LAP at high concentrations for BTE purposes remains feasible. The in vivo analysis also found that the high concentration of LAP can significantly accelerate bone tissue formation and enhance the bioactivity of polymer-based scaffolds, demonstrating its potential as a promising indicator for new approaches in the construction of biomimetic grafts.

Acknowledgments

A.O.L thank to CNPq (403890/2023-3 and 310883/2020-2). F.R.M. thank to CNPq (311531/2020-2).

Disclosure

The authors and institutions declare no financial interest or benefit from the work presented in this manuscript. The authors declare no competing financial interest.

References

1. Liang Y, Wang X, Wu J, Qiu X, Jiang X, Huang C. Poly (ε-caprolactone) scaffold functionalized with hyaluronic acid and gelatin by coaxial electrospraying for cartilage tissue engineering. *Polymers*. 2021;13(24):4442. doi:10.3390/polym13244442
2. Budharaju H, Suresh S, Sekar MP, et al. Ceramic materials for 3D printing of biomimetic bone scaffolds – current state-of-the-art & future perspectives. *Mater Des*. 2023;231:112064. doi:10.1016/j.matdes.2023.112064
3. Ma Z, He H, Deng C, et al. 3D bioprinting of proangiogenic constructs with induced immunomodulatory microenvironments through a dual cross-linking procedure using Laponite® incorporated bioink. *Composites Part B*. 2022;229:109399. doi:10.1016/j.compositesb.2021.109399
4. Dong L, Bu Z, Xiong Y, et al. Facile extrusion 3d printing of gelatine methacrylate/laponite® nanocomposite hydrogel with high concentration nanoclay for bone tissue regeneration. *Int J Biol Macromol*. 2021;188:72–81. doi:10.1016/j.ijbiomac.2021.07.199
5. Li T, Liu ZL, Xiao M, et al. Impact of bone marrow mesenchymal stem cell immunomodulation on the osteogenic effects of Laponite®. *Stem Cell Res Ther*. 2018;9:100. doi:10.1186/s13287-018-0818-0
6. Chen Y, Lin Y, Chen X, Zhang J, Lin X, Chen G. Cell-loaded injectable gelatin/alginate/LAPONITE® nanocomposite hydrogel promotes bone healing in a critical-size rat calvarial defect model. *RSC Adv*. 2020;10(28):16827–16835. doi:10.1039/D0RA03040F
7. Rogowska-Tylman J, Locs J, Salma I, et al. In vivo and in vitro study of a novel nanohydroxyapatite sonocoated scaffolds for enhanced bone regeneration. *Mater Sci Eng*. 2019;99:669–684. doi:10.1016/j.msec.2019.01.084
8. Magalhães LSSM, Andrade DB, Bezerra RDS, et al. Nanocomposite hydrogel produced from PEGDA and laponite® for bone regeneration. *J Funct Biomater*. 2022;13(2):53. doi:10.3390/jfb13020053
9. Myeroff C, Archdeacon M. Autogenous bone graft: donor sites and techniques. *J Bone Joint Surg*. 2011;93(23):2227–2236. doi:10.2106/JBJS.J.01513
10. Gómez S, Vlad MD, López J, Fernández E. Design and properties of 3D scaffolds for bone tissue engineering. *Acta Biomater*. 2016;42:341–350. doi:10.1016/j.actbio.2016.06.032
11. Bose S, Roy M, Bandyopadhyay A. Recent advances in bone tissue engineering scaffolds. *Trends Biotechnol*. 2012;30(10):546–554. doi:10.1016/j.tibtech.2012.07.005
12. Shin M, Yoshimoto H, Vacanti JP. In vivo bone tissue engineering using mesenchymal stem cells on a novel electrospun nanofibrous scaffold. *Tissue Eng*. 2004;10(1–2):33–41. doi:10.1089/107632704322791673
13. Oliveira JE, Mattoso LHC, Orts WJ, Medeiros ES. Structural and morphological characterization of micro and nanofibers produced by electrospinning and solution blow spinning: a comparative study. *Adv Mater Sci Eng*. 2013;2013:409572. doi:10.1155/2013/409572
14. Badrossamay MR, Balachandran K, Capulli AK, et al. Engineering hybrid polymer-protein super-aligned nanofibers via rotary jet spinning. *Biomaterials*. 2014;35(10):3188–3197. doi:10.1016/j.biomaterials.2013.12.072
15. Jakus AE, Rutz AL, Jordan SW, et al. Hyperelastic "bone": a highly versatile, growth factor–free, osteoregenerative, scalable, and surgically friendly biomaterial. *Sci Transl Med*. 2016;8(358):358ra127–358ra127. doi:10.1126/scitranslmed.aaf7704
16. Cidonio G, Alcala-Orozco CR, Lim KS, et al. Osteogenic and angiogenic tissue formation in high fidelity nanocomposite Laponite®-gelatin bioinks. *Biofabrication*. 2019;11(3):035027. doi:10.1088/1758-5090/ab19fd

17. Liu B, Li J, Lei X, et al. Cell-loaded injectable gelatin/alginate/LAPONITE® nanocomposite hydrogel promotes bone healing in a critical-size rat calvarial defect model. *RSC Adv*. 2020;10(43):25652–25661. doi:10.1039/D0RA03040F
18. Ullah A, Haider MK, Wang F, et al. "Clay-corn-caprolactone" a novel bioactive clay polymer nanofibrous scaffold for bone tissue engineering. *Appl Clay Sci*. 2022;220:106455. doi:10.1016/j.clay.2022.106455
19. Xu X, Xiao L, Xu Y, et al. Vascularized bone regeneration accelerated by 3D-printed nanosilicate-functionalized polycaprolactone scaffold. *Regen Biomater*. 2021;8(6):rbab061. doi:10.1093/rb/rbab061
20. Chen H, Khong J, Huang J. Direct ink writing of polycaprolactone/laponite® composite for bone implants: 3d characterization using x-ray micro ct. *Orthop Proc*. 2021;103-B(SUPP_16):74. doi:10.1302/1358-992X.2021.16.074
21. Soleimani M, Nadri S. A protocol for isolation and culture of mesenchymal stem cells from mouse bone marrow. *Nat Protoc*. 2009;4:102–106. doi:10.1038/nprot.2008.221
22. International Organization For Standardization, Biological evaluation of medical devices. *Part 5: Tests for cytotoxicity: in vitro methods", 3st ed, ISO 10993-5*, 2009.
23. Balani SB, Ghaffar SH, Chougan M, et al. Processes and materials used for direct writing technologies: a review. *Results Eng*. 2021;11:100257. doi:10.1016/j.rineng.2021.100257
24. Khajehmohammadi M, Azizi Tafti R, Nikukar H. Effect of porosity on mechanical and biological properties of bioprinted scaffolds. *J Biomed Mater Res*. 2023;111(2):245–260. doi:10.1002/jbm.a.37455
25. Tabesh E, Kharaziha M, Mahmoudi M, et al. Biological and corrosion evaluation of Laponite: poly (caprolactone) nanocomposite coating for biomedical applications. *Colloids Surf A*. 2019;583:123945. doi:10.1016/j.colsurfa.2019.123945
26. Xu X, Zhuo J, Xiao L, et al. Nanosilicate-functionalized polycaprolactone orchestrates osteogenesis and osteoblast-induced multicellular interactions for potential endogenous vascularized bone regeneration. *Macromol biosci*. 2022;22(2):2100265. doi:10.1002/mabi.202100265
27. López-Angulo D, Bittante AMQB, Luciano CG, et al. Effect of laponite® on the structure, thermal stability and barrier properties of nanocomposite gelatin films. *Food Bioscience*. 2020;35:100596. doi:10.1016/j.fbio.2020.100596
28. Cunha VRR, Lima FCDA, Sakai VY, et al. LAPONITE®-pilocarpine hybrid material: experimental and theoretical evaluation of pilocarpine conformation. *RSC Adv*. 2017;7(44):27290–27298. doi:10.1039/C7RA01841G
29. Ghadiri M, Chrzanowski W, Lee WH, et al. Physico-chemical, mechanical and cytotoxicity characterizations of laponite®/alginate nanocomposite. *Appl Clay Sci*. 2013;85:64–73. doi:10.1016/j.clay.2013.08.049
30. Baptista R, Guedes M. Morphological and mechanical characterization of 3D printed PLA scaffolds with controlled porosity for trabecular bone tissue replacement. *Mater Sci Eng*. 2022;118:111528. doi:10.1016/j.msec.2020.111528
31. Cipitria A, Skelton A, Dargaville TR, Dalton PD, Hutmacher DWD. Fabrication and characterization of pcl electrospun scaffolds—a review. *J Mater Chem*. 2011;21(26):9419. doi:10.1039/c0jm04502k
32. Wu C-J, Gaharwar AK, Schexnailder PJ, et al. Development of biomedical polymer-silicate nanocomposites: a materials science perspective. *Materials*. 2010;3(5):2986–3005. doi:10.3390/ma3052986
33. Pitt CG, Chasalow FI, Hibionada YM, Klimas DM, Schindler A. Aliphatic polyesters. I. The degradation of poly(ϵ-caprolactone) in vivo. *J Appl Polym Sci*. 1981;26(11):3779–3787. doi:10.1002/app.1981.070261124
34. Gautam G, Kumar S, Kumar K. Processing of biomaterials for bone tissue engineering: state of the art. *Mater Today Proc*. 2022;50:2206–2217. doi:10.1016/j.matpr.2021.09.459
35. Woodruff MA, Hutmacher DW. The return of a forgotten polymer—polycaprolactone in the 21st century. *Prog Polym Sci*. 2010;35(10):1217–1256. doi:10.1016/j.progpolymsci.2010.04.002
36. Zeqian X, Xuanyu Q, Bao M, et al. Biomineralization inspired 3D printed bioactive glass nanocomposite scaffolds orchestrate diabetic bone regeneration by remodeling micromilieu. *Bioact Mater*. 2023;25:239–255. doi:10.1016/j.bioactmat.2023.01.024
37. Silva MCS, Sousa GF, Santana MV, Tsumura WG, Stocco TD, Lobo AO. Tailoring mechanical properties of printed GelMA scaffolds with multilayers of PLA/Laponite® nanocomposite fibers. *Mater Lett*. 2024;364:136314. doi:10.1016/j.matlet.2024.136314
38. Gaharwar AK, Mukundan S, Karaca E, et al. Nanoclay-enriched poly(ε-Caprolactone) electrospun scaffolds for osteogenic differentiation of human mesenchymal stem cells. *Tissue Eng Part A*. 2014;20(15–16):2088–2101. doi:10.1089/ten.tea.2013.0281
39. Da Fonseca GF, Avelino SDOM, Mello DDCR, e colab. Scaffolds of PCL combined to bioglass: synthesis, characterization and biological performance. *J Mater Sci*. 2020;31(5):41. doi:10.1007/s10856-020-06382-w
40. Camarero-Espinosa S, Moroni L. Janus 3D printed dynamic scaffolds for nanovibration-driven bone regeneration. *Nat Commun*. 2021;12(1):1031. PMID: 33589620; PMCID: PMC7884435. doi:10.1038/s41467-021-21325-x
41. Ibrahim DM, Sani ES, Soliman AM, et al. Bioactive and elastic nanocomposites with antimicrobial properties for bone tissue regeneration. *ACS Appl Bio Mater*. 2020;3(5):3313–3325. doi:10.1021/acsabm.0c00250
42. Hasibuan PAZ. Antimicrobial and antihemolytic properties of a CNF/AgNP-chitosan film: a potential wound dressing material. *Heliyon*. 2021;7(10). doi:10.1016/j.heliyon.2021.e08197
43. Arif ZU, Khalid MY, Noroozi R, Sadeghianmaryan A, Jalalvand M, Hossain M. Recent advances in 3D-printed polylactide and polycaprolactone-based biomaterials for tissue engineering applications. *Int J Biol Macromol*. 2022;218:930–968. doi:10.1016/j.ijbiomac.2022.07.140
44. Stallmann HP, Roo de R, Faber C, Amerongen AVN, Wuisman PIJM. In vivo release of the antimicrobial peptide HLF1-11 from calcium phosphate cement. *J Orthop Res*. 2008;26(4):531–538. doi:10.1002/jor.20511
45. Kamiloglu S, Sari G, Ozdal T, Capanoglu E. Guidelines for cell viability assays. *Food Front*. 2020;1(3):332–349. doi:10.1002/fft2.44
46. Andrade TM, Mello DCR, Elias CMV, et al. In vitro and in vivo evaluation of rotary-jet-spun poly(ε-Caprolactone) with high loading of nano-hydroxyapatite. *J Mater Sci Mater Med*. 2019;30(2):19. doi:10.1007/s10856-019-6222-1
47. Mihaila SM, Gaharwar AK, Reis RL, Khademhosseini A, Marques AP, Gomes ME. The osteogenic differentiation of SSEA-4 sub-population of human adipose derived stem cells using silicate nanoplatelets. *Biomaterials*. 2014;35(33):9087–9099. doi:10.1016/j.biomaterials.2014.07.052
48. Cao B, Lin J, Tan J. 3D-printed vascularized biofunctional scaffold for bone regeneration. *IJB*. 2023;9(3):702. doi:10.18063/ijb.702
49. Rodrigo MJ, Cardiel MJ, Fraile JM, Mayoral JA, Pablo LE, Garcia-Martin E. Laponite® for biomedical applications: an ophthalmological perspective. *Mater Today Bio*. 2024;24:100935. doi:10.1016/j.mtbio.2023.100935

50. Arab-Ahmadi S, Irani S, Bakhshi H, Ghalandari B. Immobilization of carboxymethyl chitosan/Laponite® on polycaprolactone nanofibers as osteoinductive bone scaffolds. *Polym Adv sTechnol*. 2021;32. doi:10.1002/pat.5128
51. He M, Li L, Liu Y, et al. Decellularized extracellular matrix coupled with polycaprolactone/laponite to construct a biomimetic barrier membrane for bone defect repair. *Int J Biol Macromol*. 2024;276:133775. doi:10.1016/j.ijbiomac.2024.133775
52. Li Y, Zhao D, Wang Z, et al. Minimally invasive bone augmentation through subperiosteal injectable hydroxylapatite/laponite/alginate nanocomposite hydrogels. *Int J Biol Macromol*. 2023;231:123232. doi:10.1016/j.ijbiomac.2023.123232
53. Saygili E, Saglam-Metiner P, Cakmak B, et al. Bilayered laponite/alginate-poly(acrylamide) composite hydrogel for osteochondral injuries enhances macrophage polarization: an in vivo study. *Biomater Adv*. 2022;134:112721. doi:10.1016/j.msec.2022.112721
54. Tavoni M, Dapporto M, Tampieri A, Sprio S. Bioactive calcium phosphate-based composites for bone regeneration. *J Compos Sci*. 2021;5:227. doi:10.3390/jcs5090227
55. Miroshnichenko LA, Polyakova TY, Litvinova LS, et al. Review of local cellular and molecular processes of bone tissue regeneration induced by calcium phosphate materials. *Cell Tiss Biol*. 2024;18:148–162. doi:10.1134/S1990519X23700062
56. Orafa Z, Irani S, Zamanian A, Bakhshi H, Nikukar H, Ghalandari B. Coating of laponite® on PLA nanofibrous for bone tissue engineering application. *Macromol Res*. 2021;29(3):191–198. doi:10.1007/s13233-021-9028-1
57. Wang Z, Hu J, Yu J, Chen D. Preparation and characterization of nano-laponite®/PLGA composite scaffolds for urethra tissue engineering. *Mol Biotechnol*. 2020;62(3):192–199. doi:10.1007/s12033-020-00237-z